Towards CARS Endoscopy

François Légaré*

Center for Nanoscale Systems and Department of Chemistry and Chemical Biology, Harvard University, 12 Oxford Street, Cambridge, MA 02138

Conor L. Evans*, Feruz Ganikhanov, and X. Sunney Xie

Department of Chemistry and Chemical Biology,
Harvard University, 12 Oxford Street, Cambridge, MA 02138
xie@chemistry.harvard.edu

** These authors contributed equally.*

Abstract: We provide a proof-of-principle demonstration of CARS endoscopy. The design utilizes a single mode optical fiber with a focusing unit attached to the distal end. Picosecond pump and Stokes pulse trains in the near infrared are delivered through the fiber with nearly unaltered spectral and temporal characteristics at intensities needed for endoscopy. CARS endoscopic images are recorded by collecting the epi-CARS signal generated at the sample and raster scanning the sample with respect to the fiber. This CARS endoscope prototype represents an important step towards *in situ* chemically selective imaging for biomedical applications.

OCIS code: (170.2150) Endoscopic imaging; (190.4380) Nonlinear optics, four-wave mixing; (300.6230) Spectroscopy, coherent anti-Stokes Raman scattering.

References and links

1. J.-X. Cheng and X. S. Xie, " Coherent anti-Stokes Raman scattering microscopy: instrumentation, theory and applications ," J. Phys. Chem. B **108**, 827 (2004).
2. J.-X. Cheng, L. Book, and X. S. Xie, "Polarization coherent anti-Stokes Raman scattering microscopy," Opt. Lett. **26**, 1341 (2001).
3. A. Volkmer, L. Book, and X. S. Xie, "Time-resolved coherent anti-Stokes Raman scattering microscopy: Imaging based on Raman free induction decay," Appl. Phys. Lett. **80**, 1505 (2002).
4. A. Volkmer, J.-X. Cheng, and X. Sunney Xie, "Vibrational imaging with high sensitivity via epi-detected coherent anti-Stokes Raman scattering microscopy," Phys. Rev. Lett. **87**, 23901 (2001).
5. E. O. Potma, C. L. Evans, and X. S. Xie, "Heterodyne coherent anti-Stokes Raman scattering (CARS) imaging," Opt. Lett. **31**, 241 (2006).
6. F. Ganikhanov, C. L. Evans, B. G. Saar, and X. S. Xie, "High sensitivity vibrational imaging with frequency modulation coherent anti-Stokes Raman scattering (FM CARS) microscopy," Opt. Lett. **31** (2006). In Press.
7. J.-X. Cheng, K. Y. Jia, G. Zheng, and X. S. Xie, "Laser-scanning coherent anti-Stokes Raman scattering microscopy and applications to Cell Biology," Biophys. J. **83**, 502 (2002).
8. H. Wang, Y. Fu, P. Zickmund, R. Shi, and J.-X. Cheng, "Coherent anti-Stokes Raman scattering imaging of Axonal Myelin in live spinal tissues," Biophys. J. **89**, 581 (2005).
9. C. L. Evans, E. O. Potma, M. Poureshagh, D. Coté, C. L. Lin, and X. S. Xie, "Molecular imaging of tissue in vivo with video-rate coherent anti-Stokes Raman scattering (CARS) microscopy," PNAS **102**, 16808 (2005).
10. F. Ganikhanov, S. Carrasco, M. Katz, W. Seitz, D. Kopf, and X. S. Xie, "A Broadly tunable dual-wavelength light source for CARS Microscopy," Opt. Lett. **31**, 1292 (2006).
11. F. Légaré, F. Ganikhanov, and X. S. Xie, "Towards an integrated coherent anti-Stokes Raman scattering (CARS) microscopy system," Proc. SPIE **5971**, 35 (2005).
12. G. J. Tearney, M. E. Brezinski, B. E. Bouma, S. A. Boppart, C. Pitris, J. F. Southern, and J. G. Fujimoto, "In Vivo Endoscopic Optical Biopsy with Optical Coherence Tomography," Science **276**, 2037 (1997).
13. B. A. Flusberg, E. D. Cocker, W. Piyawattanametha, J. C. Jung, E. L. M. Cheung, and M. J. Schnitzer, "Fiber-optic fluorescence imaging," Nat. Methods **12**, 941 (2005).
14. J. C. Jung and M. J. Schnitzer, "Multiphoton Endoscopy," Opt. Lett. **28**, 902 (2003).
15. M. T. Myaing, D. J. MacDonald, and X. Li, "Fiber-optic scanning two-photon fluorescence endoscope," Opt. Lett. **31**, 1076 (2006).

#69842 - $15.00 USD Received 10 April 2006; revised 27 April 2006; accepted 27 April 2006

16. L. Fu, A. Jain, H. Xie, C. Cranfield, and M. Gu, "Nonlinear optical endoscopy based on a double-clad photonic crystal fiber and a MEMS mirror," Opt. Express **14**, 1027 (2006).
17. A. Yariv, *Optical Electronics in Modern Communications* (Oxford University Press, New York, 1997), pp. 101.
18. R.W. Boyd, *Nonlinear Optics* (Academic Press, London, 2003), pp. 356-358.
19. Y. Silberberg and I. Bar-Joseph, "Optical instabilities in a nonlinear Kerr medium," J. Opt. Soc. Am. B **1**, 662-670 (1984).
20. J.-X. Cheng, A. Volkmer, and X. S. Xie, "Theoretical and experimental characterization of coherent anti-Stokes Raman scattering microscopy," JOSA B **19**, 1363 (2002).
21. V. V. Yakovlev and G. I. Petrov, " Enhancing red-shifted white-light continuum generation in optical fibers for applications in nonlinear Raman microscopy," **13**, 1299 (2005)

1. Introduction

Coherent anti-Stokes Raman scattering (CARS) microscopy has been demonstrated as a powerful tool for label-free optical imaging that offers many advantages including (i) chemical contrast based on Raman vibrational activity, (ii) high sensitivity and rapid acquisition rates due to the coherent nature of the CARS process, (iii) and sub-wavelength lateral spatial resolution [1]. As CARS is a nonlinear process, the signal is generated at the laser focus, enabling point-by-point three-dimensional imaging. Over the past several years, various detection schemes have been developed for CARS microscopy, including polarization selective [2], time resolved [3], epi-detected [4], heterodyne detected [5], and frequency modulation CARS [6] in order to improve the sensitivity and selectivity. CARS microscopy has been successfully applied to cellular [7] and tissue [8,9] imaging.

CARS requires two laser frequencies called "pump" (ω_p) and "Stokes" (ω_s). When the pump and Stokes difference frequency, $\Delta\omega = \omega_p - \omega_s$, is set to that of a vibrational resonance, Ω, a strong optical response occurs at the "anti-Stokes" frequency, $\omega_{as} = 2\omega_p - \omega_s$ [Fig 1(a)]. The CARS signal is derived from the third-order nonlinear susceptibility, $\chi^{(3)}$, of a material, which is significantly enhanced when the difference frequency is tuned into a resonance. As a nonlinear process, CARS requires high peak-powers for efficient signal generation. Tunable picosecond laser sources are optimal for CARS imaging applications as they achieve high spectral resolution and optimal signal to background ratios [1]. Synchronously pumped and broadly tunable optical parametric oscillators (OPOs) [10] are ideal sources for this purpose. For such laser sources, it is possible to deliver the beams to a microscope through 1 meter of single-mode fiber without affecting the temporal and spectral domain characteristics [11].

For many applications in biomedicine, it is desirable to perform tissue imaging *in situ*. Endoscopy, in particular, has been widely used in medicine for applications ranging from surgical interventions to disease diagnosis. Recent advances in endoscopic techniques have utilized contrast based on optical coherence tomography (OCT) [12], one and two-photon fluorescence [13-16], and second harmonic generation [16], leading to immediate applications in clinical environments. While OCT has been very successful for imaging tissue morphology, its contrast is solely based on refractive index differences. Endogenous fluorescence endoscopy is only sensitive to intrinsic biological fluorophores, which limits its applications. Second harmonic endoscopy is extremely sensitive to non-centrosymmetric structures, but few biological materials have this optical property. An endoscope based on the vibrational contrast of CARS would offer label-free chemically-selective imaging *in situ*, making it an ideal tool for biomedical applications. In this report, we present a prototype CARS endoscope capable of imaging specimens with submicron lateral resolution and ~12 μm axial resolution.

2. Experimental set up

2.1. Tunable laser source

Figure 1(b) shows a schematic of the proof-of-principle CARS endoscope system. The laser source consisted of a passively mode-locked 10W Nd:YVO_4 laser (High-Q Laser GmbH) operating at 1064nm, which delivered transform-limited 7ps pulses at a repetition rate of

#69842 - $15.00 USD Received 10 April 2006; revised 27 April 2006; accepted 27 April 2006

76MHz. The majority of the Nd:YVO_4 output (9W) was used to synchronously pump an OPO (APE-Berlin). The OPO cavity was configured to resonate on its signal wavelength and utilized intracavity-doubling to efficiently generate a 5ps pulse train with up to 2W of average output power. A broad tuning range of 780-920nm was achieved by adjusting the position and temperature of a multi-grating, periodically poled lithium niobate crystal used for parametric generation. A portion of the 1064nm output (1.5W) was used as a Stokes beam while the tunable OPO output provided the pump beam. The output beam quality of the pump and Stokes sources was estimated to be M^2 ~1.3 and ~1.1, respectively. The pump and Stokes beams were combined on a dichroic mirror (Chroma, 950DCXR) and directed to coupling optics at the proximal fiber end.

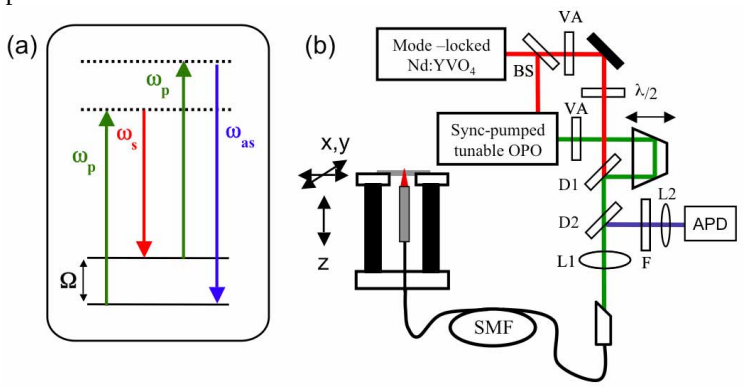

Fig. 1. (a) CARS energy diagram. (b) Experimental setup: BS, 15% beam splitter; VA, variable attenuator; λ/2, half-waveplate; D1, 950nm longpass dichroic mirror; D2, 750nm longpass dichroic mirror; F, three 670nm bandpass filters; L1, aspheric lens; L2, 10cm concave lens.

2.2. Endoscope design

The combined pump and Stokes beam was coupled by an aspheric lens into a 1m-long step index, non-polarization maintaining silica fiber designed for single mode propagation at 830nm (0.12 numerical aperture, 5.6μm mode field diameter). The fiber bandwidth allowed for single mode propagation up to 200nm above the designed wavelength, enabling efficient propagation of the pump and Stokes frequencies. Since the fiber was able to efficiently propagate a wide range of pump wavelengths, the endoscope could easily be used to probe any biologically relevant Raman active vibrational resonance. The size and divergence of the pump and Stokes beams were independently adjusted before the dichroic mirror to maximize the coupling efficiency. A delay line in the pump beam line was used to overlap the pump and Stokes pulse trains in time. The fiber was found to cause a wavelength-dependent polarization rotation, which is undesirable since the maximum CARS signal is generated when the pump and Stokes polarizations are the same [2]. A half-wave plate in the Stokes beam line was used to compensate for this polarization rotation.

Straight fiber terminals were found to cause significant optical feedback to the Nd:YVO_4 laser, necessitating the use of angle-cut fiber terminations. The typical coupling efficiency of the beams into the fiber was better than 40%. A 4mm diameter focusing unit utilizing an aspheric lens (2.4mm diameter, 0.43 numerical aperture, 1.1mm working distance) was attached to the distal fiber tip. Samples were raster scanned by a three-dimensional piezo stage (PI, P547.3CL) with respect to the fixed fiber assembly. The backward-propagating (epi) CARS photons generated in focus were collected by the focusing unit and separated from the excitation beams at the proximal fiber end with a dichroic mirror (Chroma, 750DCXR). The CARS signal was filtered with three 670nm bandpass filters (Ealing 42-7393) and focused with a 100mm concave lens onto an avalanche photodiode (PerkinElmer, SPCM-AQR-14).

#69842 - $15.00 USD Received 10 April 2006; revised 27 April 2006; accepted 27 April 2006

3. Results

3.1. Pump and Stokes pulse propagation in fiber

The temporal characteristics for both pulses were precisely estimated using the material dispersion, modal refractive index, and nonlinear optical parameters for a fused silica fiber. Temporal broadening for the 5-7 picosecond transform-limited pulses in the 1m-length fiber was negligible and estimated to be less than 0.1% using the well-known formula for pulse temporal broadening in dispersive media [17]. Auto- and cross-correlation traces for the two pulses [Fig. 2(a)] confirmed this prediction.

Pulse spectral broadening due to fiber propagation can potentially have a large effect on the spectral resolution and image contrast of the CARS endoscope [1]. Spectral broadening due to self-phase modulation begins to be noticeable when the nonlinear phase shift becomes close to 2π. The per-pulse energy corresponding to this condition is found to be:

$$E_{2\pi} \approx \frac{\pi \lambda t_p D_{eff}^2}{4 n_2 L} \tag{1}$$

where t_p is the pulsewidth (~6ps), D_{eff} is the mode field diameter (5.6 μm), n_2 is the nonlinear refractive index of silica (2.6×10^{-16}cm^2/W), and L is the fiber length [18]. For a fiber length of 1m and a pulse wavelength centered at 800nm, the 2π-shift occurs at pulse energies of nearly 4nJ, which is equivalent to approximately 300mW average power at a repetition rate of 76MHz. Measured power spectra of the pump and Stokes pulse trains before and after propagation through different fiber lengths are presented in figures 2(b) and 2(c).

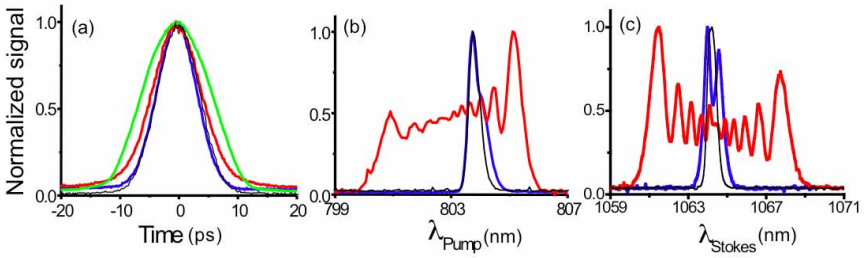

Fig. 2. (a) Autocorrelation traces of pump (blue) and Stokes (red) pulses after propagation in 1m long fiber. Cross-correlation trace after 1m of fiber propagation (green). The faintly seen black trace is the autocorrelation of the pump before fiber propagation. Measured pump (b) and Stokes (c) power spectra after the OPO (black), 1m- (blue) and 5m- red) long fiber propagation at 400mW and 700mW of pump and Stokes fiber output, respectively . The fiber input powers were 1W and 1.3W, respectively.

The 2π nonlinear phase shift was observed at average powers of 400mW and 700mW for 803.5nm and 1064nm, respectively [Figs. 2(b) and 2(c), blue traces]. When collecting endoscopic images, we typically used 80mW of power for both laser beams. These average powers are so far below the threshold for self-phase modulation that the pump and Stokes spectra do not undergo detectable broadening. Therefore, at the powers used, fiber propagation does not affect the CARS spectral selectivity [11].

The use of longer fibers, however, can result in noticeable spectral broadening. Propagation through 5m of fiber resulted in spectral broadening of 40cm^{-1} and 60cm^{-1} for 400mW of 803.5nm and 700mW of 1064nm, respectively [Figs. 2(b) and (c), red traces]. This broadening is small and on the same order as characteristic Raman linewidths in liquids.

The peak power of the oscillators used in this experiment was over three orders of magnitude lower than the critical power for beam self-focusing [18]. This agrees with our observation of perfect TEM_{00} mode intensity profiles with no signs of beam filamentation. The two-beam coupling effect [19] (gain of the 'Stokes' beam in the presence of the 'pump'

#69842 - $15.00 USD Received 10 April 2006; revised 27 April 2006; accepted 27 April 2006

in this case) was not observed due to the instantaneous electronic response time of Kerr nonlinearity in silica.

3.2. Endoscopic imaging

We characterized the performance of the prototype CARS endoscope by imaging size-calibrated polystyrene beads with the pump and Stoke difference frequency set to the aliphatic symmetric CH_2 stretch ($\Delta\omega$=2845cm^{-1}). Figure 3(a) shows an XY image of 0.75μm polystyrene beads spin-coated on a coverslip. A Gaussian fit to the bead profile gives a FWHM of 0.76μm. Smaller beads (0.5μm) were found to have the same FWHM profile, indicating an upper bound on the lateral resolution of approximately 0.8μm. The axial resolution upper bound was measured to be ~12μm using the same procedure. This spatial resolution was expected based on the numerical aperture of the focusing lens and is sufficient for imaging tissue morphology.

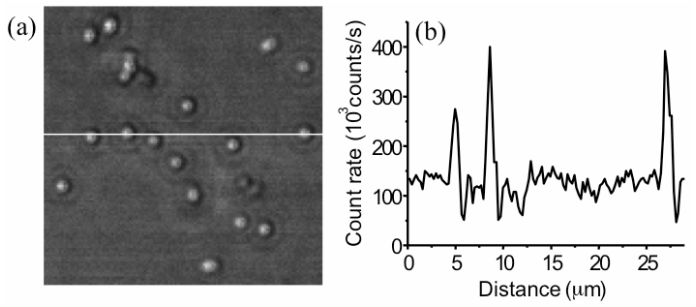

Fig. 3. (a) Prototype CARS endoscope image of 0.75μm polystyrene beads embedded in agarose gel spin-coated on a coverslip ($\Delta\omega$=2845cm^{-1}). The image dimension is 29μm×29μm (128×128 pixels). The pump and Stokes powers at the sample were 80mW each, with a pixel dwell time of 1ms. (b) CARS intensity profile along the white line in (a). The CARS contrast decreased when the system was tuned off the resonance maximum.

The prototype endoscope collects epi-CARS signals, which can come from three different mechanisms [1, 9]. In the first mechanism, epi-signal is generated from objects that are comparable in size to the excitation wavelengths. In the second mechanism, epi-CARS is generated at the interface of two media with different third-order nonlinear susceptibilities. For these two mechanisms, the epi-CARS signal arises from incomplete destructive interference in the epi-direction [1, 20]. A third mechanism can occur in thick samples (> 100μm); multiple scattering events due to the turbidity of the specimen can redirect a fraction of the intense forward-propagating CARS signal in the epi-direction. This mechanism has been shown to generate the dominant epi-CARS signal in tissues such as skin [9].

Thus, for small objects such as the 0.75μm-diameter beads in figure 3, the epi-CARS signal arose solely from the first mechanism. For larger objects such as the 5μm beads in figure 4, however, the second epi-CARS mechanism dominated signal generation. Epi-signal generated at the bead surface caused the larger beads to have a ring-shaped appearance. The center of the bead did not contribute to the image since it can be considered as bulk material in which complete destructive interference occurred in the epi-direction. The lower-intensity ring features in figure 4 arose from out-of-focus beads.

To mimic imaging thick tissue, we attempted to detect the backscattered forward-CARS due to the third epi-CARS mechanism from intralipid tissue phantoms [9]. Although strong forward-CARS signal was redirected backwards, the signal could not be detected with the endoscope because the multiple scattering events occurred outside the focal volume. The single-mode fiber, acting like a confocal pinhole [13], rejected photons scattered in the epi-direction from outside the focal plane. Thus, our current prototype can only collect epi-CARS resulting from the first two mechanisms. For CARS endoscopy to be most useful for tissue

#69842 - $15.00 USD Received 10 April 2006; revised 27 April 2006; accepted 27 April 2006

imaging, future endoscope designs will need to collect the backscattered CARS signal. Since the backscattered signal is typically orders of magnitude more intense than epi-CARS arising from incomplete destructive interference alone, such endoscope designs will likely require lower excitation powers and could operate at greater acquisition rates.

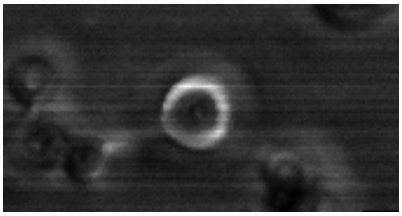

Fig. 4. Prototype CARS endoscope image of 5μm polystyrene beads embedded in agarose spin-coated on a coverslip ($\Delta\omega$=2845cm^{-1}). The ring-like structure is due to signal arising at the edge of the bead from incomplete destructive interference in the epi-direction. The image dimension is 31μm×15μm (139×66 pixels). The pixel dwell time was 1ms.

In this report, we scanned the sample relative to a fixed focus in order to demonstrate delivery and detection through the same fiber. This successful demonstration paves the way for an endoscope that incorporates a distal fiber scanning mechanism [13-16]. Our proof-of-principle endoscope coupled with such a scanning mechanism would be extremely useful for imaging samples for which the first and second epi-CARS mechanisms dominate, such as nerve bundles [8].

In order to minimize the size of the focusing unit, our CARS endoscope prototype utilized a low numerical aperture focusing lens. This differs from CARS microscopes, which normally utilize achromatic high numerical aperture objectives that give higher spatial resolution, signal generation, and collection efficiency. For epi-signal generated through the first two mechanisms, the performance of the endoscope is expected to be the same as that of a CARS microscope equipped with a similar numerical aperture focusing unit. Since the aspheric lens in our prototype has chromatic aberrations, the spatial overlap of the pump and Stokes can be further optimized for efficient signal generation. The collection efficiency of the anti-Stokes signal is also affected by the chromaticity. An achromatic focusing unit is expected to significantly improve endoscope performance.

It is worth noting that the spectral broadening associated with long fiber length propagation could be used for endoscopic multiplex CARS microspectroscopy [21]. This could be realized, for example, by propagating the Stokes laser pulse train at higher average powers through the fiber while reducing the pump power.

4. Conclusion

We have demonstrated a proof-of-principle CARS endoscope using a single mode fiber for the simultaneous delivery of the pump and Stokes beams and the collection of the anti-Stokes signal. Fiber propagation did not cause significant change to the pump and Stokes temporal and spectral profiles at powers necessary for endoscopy. The imaging contrast is the result of CARS signal generated due to incomplete destructive interference in the epi-direction. This achievement, together with future developments such as backscattered photon collection and distal fiber scanning, bring us closer to a CARS endoscope capable of label-free *in situ* biomedical imaging.

Acknowledgments

This work is funded by an NIH Director's Pioneer Award to X.S.X. The authors thank Dr. Silvia Carrasco for her helpful suggestions. F. L. thanks NSERC (Natural Sciences and Engineering Research Council of Canada) for grants supporting the present research.

#69842 - $15.00 USD Received 10 April 2006; revised 27 April 2006; accepted 27 April 2006